# Tropical thermocline helps power Pacific equatorial upwelling

Noel G. Brizuela[a] , Chia-Ying Lee[a] , Adam H. Sobel[a,b] , Richard Seager[a] , Suzana J. Camargo[a] , Jing-Yi Zhuo[a]

[a] *Lamont-Doherty Earth Observatory, Columbia University, New York, NY, USA*

[b] *Department of Applied Physics and Applied Mathematics, Columbia University, New York, NY, USA*



*Corresponding author*: Noel G. Brizuela, noelgb@ldeo.columbia.edu

ABSTRACT: Upwelling in the equatorial Pacific Ocean exerts a primary influence on the Earth's climate, but there is great uncertainty on whether this influence will intensify or weaken under global warming. The dominant dynamical theory of equatorial upwelling argues that the easterly trade winds 'pull' water up towards the surface via Ekman suction. In contrast, studies of decadal variability suggest that the subtropical cells 'push' equatorial upwelling from below. Therefore, it is unclear whether upwelling is 'pulled from above' by Ekman divergence or 'pushed from below' by geostrophic convergence. Here, we use a framework of local available energetics to study the Pacific shallow overturning circulation and find that at least 20-50% of equatorial upwelling cannot be powered directly by winds along the equator, as commonly understood. Instead, this fraction of upwelling is powered by potential energy that is transferred to the thermocline via off-equatorial downwelling and diabatic processes. Water parcels holding excess potential energy in the equatorial thermocline are able to upwell without additional energy input, such that equatorial upwelling can in fact be pushed from below. The strength of this push is largely set by the trade winds, but may also be influenced by energy sources across the subtropical ocean. Unlike previous available energetics analyses of the equatorial region, our study uses complete local conservation laws that allow us to trace all energy sources and pathways. This makes our dynamical formulation particularly useful to explain variations in equatorial Pacific upwelling at interannual and decadal timescales alike.

## 1. Introduction

Upwelling in the equatorial Pacific Ocean sets the zonal sea surface temperature (SST) gradient that regulates the tropical atmospheric circulation. Therefore, variations in equatorial upwelling can induce shifts in global climate. At interannual timescales, these shifts are typically associated with fluctuations in the trade winds and the Equatorial Current System (ECS) via the Bjerknes feedback (Zebiak and Cane 1987). In turn, decadal variability is linked to equatorward flows that close the Subtropical Cells (STCs) (Luo et al. 2003; Capotondi et al. 2023). Because the ECS and STCs are inextricably connected by equatorial upwelling (Lu et al. 1998), dynamical understanding of future changes in Pacific Ocean climate requires that ECS- and STC-based views of variability are compatible.

Interactions between the STCs and the ECS are well documented, but untangling the dynamical and thermodynamical aspects of these interactions remains a challenge. One obstacle is that the ECS and STCs are thought to regulate equatorial upwelling velocities by different and seemingly unrelated mechanisms. The ECS view of equatorial upwelling has the thermocline 'pulled from above', as easterly winds drive meridional divergence in the Ekman layer (Wyrtki 1981). In contrast, Kleeman et al. (1999) suggested that speeding up of the STCs can enhance meridional convergence of thermocline flows around the equator and thus strengthen upwelling by 'pushing from below'.

Interactions between the ECS and STCs have received increased attention in recent years, as observations indicate net cooling of the cold tongue SST over past decades (Karnauskas et al. 2009). Virtually all climate models fail to accurately reproduce historical cooling in the cold tongue (Coats and Karnauskas 2017; Seager et al. 2019, 2022; Heede and Fedorov 2023). Observations stand in conflict with arguments based on air-sea flux scalings, which indicate that the cold tongue would warm at an accelerated rate under greenhouse gas forcing (Knutson and Manabe 1995; Xie et al. 2010). Likewise, model projections suggest that increased low-level moisture under global warming would weaken the Walker circulation and reduce wind-driven equatorial upwelling (Vecchi et al. 2006; Vecchi and Soden 2007). Discrepancy between historical SST trends and atmospheric arguments suggest that the observed cooling is strongly influenced by subsurface ocean processes (Clement et al. 1996; Kang et al. 2023; Hwang et al. 2024). Naturally, theories seeking to explain historical cooling invoke changes in equatorial upwelling and its effect on SST. Typically, these theories are split in two fundamental ways:

- Are climate models failing to cool the cold tongue because they upwell waters that are unrealistically warm, or because upwelling velocities are too slow?
- Are the sources of model errors relevant to the SST trend discrepancy contained in the near-equatorial region, or do errors originate in the subtropics? (Seager et al. 2019; Kang et al. 2023; Hwang et al. 2024)

It is likely that processes leading to widespread model errors are both thermal and dynamical, equatorial and off-equatorial (Heede and Fedorov 2021). However, bridging the gaps between existing theories is complicated because ECS- and STC- based explanations of equatorial upwelling are so distinct from each other. Moreover, the perception that equatorial upwelling is 'pulled from above' by equatorial easterly winds overwhelmingly dominates scientists' understanding of equatorial upwelling. Because dynamical understanding of this matter is based on mass conservation rather than vertical forces, whether upwelling can in fact be 'pushed from below,' as is necessary to support claims by Kleeman et al. (1999), is unclear. As a result, our understanding of equatorial upwelling lacks the precision and adaptability necessary to bridge ECS- and STC-based theories of Pacific variability. Ultimately, this prevents progress in explaining observed historical cooling in the cold tongue.

Previous studies have used available energetics analyses to simplify equatorial Pacific Ocean dynamics. Particular focus has been given to the relation between mechanical wind work and gravitational potential energy storage in the thermocline (Fedorov 2002; Brown and Fedorov 2008, 2010). Without precise energy conservation laws, however, such studies have mostly used energetics to describe well-known dynamics and reduce their dimensionality (Shi et al. 2020). In particular, note that the aforementioned studies only refer to basin-integrated energy, much like Lorenz (1955) and Oort et al. (1994) did for the global atmosphere and ocean respectively. Without locally-defined energy balances, the explanatory power of ocean energetics studies is drastically limited.

Here, we use a locally-defined framework of available energetics with complete conservation laws (Tailleux 2018) to trace back the energy sources that power equatorial Pacific upwelling.

By separating the contributions of kinetic and available potential energy reservoirs, we find that 20-50% of equatorial upwelling cannot be powered directly by winds along the equator, as usually understood, and instead relies on the energy of equatorward thermocline flows. We trace the majority of this energy to meridional overturning in the near-equatorial cells that downwell within 10°S and 10°N. Diabatic heating and downwelling across the STCs supply additional energy. Our findings provide a dynamical basis for the notion that equatorial upwelling can be regulated by a push from below. The framework presented here can help evaluate the ocean response to complex changes in the Walker circulation and facilitate the comparison of ECS- and STC-based theories of climate variability on interannual and decadal timescales alike.

## 2. Energetic Framework of Upwelling

Available potential energy in a stratified fluid quantifies the amount of work that can be extracted by adiabatic redistributions of fluid parcels (Lorenz 1955). This energy is usually partitioned into elastic and gravitational energy reservoirs; to define these, one needs to consider the difference in net gravitational potential energy between a fluid's actual density field ($\rho = \rho(\mathbf{x}, t)$, where $\mathbf{x} = (x, y, z)$) and a hypothetical reference state $\rho_r(z, t)$ (Holliday and Mcintyre 1981). Here, we consider equations of state under which density of seawater is determined by conservative temperature $\Theta$, salinity $S$, and pressure $p$ such that $\rho(\mathbf{x}, t) = \rho\left[\Theta(\mathbf{x}, t), S(\mathbf{x}, t), p(\mathbf{x}, t)\right]$.

There is no absolute 'right' way to derive $\rho_r$ (Tailleux 2018), but convention is that $\rho_r$ should i) result from adiabatic rearrangement of fluid parcels within the fluid volume $V_r$, and ii) approximate the fluid's state of minimum net gravitational energy, with isopycnals laying flat and stably stratified. Preserving time dependence in $\rho_r$ allows to transparently account for changes in the fluid thermodynamics that are produced by irreversible mixing as well as energy or mass fluxes across the boundaries of $V_r$ (Winters et al. 1995; Huang 1998). Given $\rho_r$, one can assign a reference depth $z_r = z_r(\mathbf{x}, t)$ to approximate the level of neutral buoyancy where a fluid parcel whose actual position is $\mathbf{x}$ would reside in the adiabatically rearranged fluid (Tailleux 2013). Thus, we seek a solution $z_r(\mathbf{x}, t)$ that meets the condition

$$\rho\left[S(\mathbf{x}, t), \Theta(\mathbf{x}, t), p(z_r)\right] = \rho_r\left[z_r(\mathbf{x}, t), t\right]. \tag{1}$$

Dependence on $S(\mathbf{x},t)$ and $\Theta(\mathbf{x},t)$ in Eq. (1) implies that seawater properties are preserved as the water parcel is virtually moved between $z$ and $z_r$. Yet, we account for the parcel's changing density as undergoes a pressure change from $p(z)$ to $p(z_r)$ (pink shading in Fig. 1). The local available gravitational potential energy density ($E_a(\mathbf{x},t)$) thus quantifies the amount of work that can be extracted from moving a water parcel away from its current depth $z$ and to its reference level $z_r$. Conversely, positive work is needed to move a water parcel away from $z_r$, much like stretching or compressing a spring away from its equilibrium position. In fact, for quasigeostrophic flow one can write

$$E_a(\mathbf{x},t) \approx -\frac{g}{2\rho_0}\frac{\partial \rho_r}{\partial z}(z-z_r)^2, \tag{2}$$

which is exactly the potential energy of a spring with the elasticity constant $-\frac{g}{\rho_0}\frac{\partial \rho_r}{\partial z}$ and equiblibrium position $z_r$, where $g$ is gravity and $\rho_0 = 1024$ kg m$^{-3}$. As for a spring, $E_a$ is definite positive and does not distinguish between downward and upward displacements of fluid parcels. Rather, $E_a$ quantifies the energy associated with deviations from $\rho_r$ (Holliday and Mcintyre 1981).

Precise treatment of $E_a$ and its conservation laws is needed to account for diabatic effects and complex stratification profiles (Huang 1998; Kang and Fringer 2010). While the quasigeostrophic approximation in Eq. (2) has been used to study equatorial Pacific dynamics before (Brown and Fedorov 2008, 2010; Brown et al. 2011), here we use the Boussinesq statement of local available energetics for diabatic compressible fluids laid out by Tailleux (2013, 2018). Given $\rho_r$ and the density $\rho(\mathbf{x},t)$ of a fluid parcel, this framework defines $E_a$ using Eq. (3). A schematic in Fig. 1 uses gray and pink shading to represent the integral in this formulation.

$$E_a(\mathbf{x},t) = \frac{g}{\rho_0}\int_{z_r}^{z} \left(\rho\left[S(\mathbf{x},t),\Theta(\mathbf{x},t),p(z')\right] - \rho_r(z',t)\right)\, dz'. \tag{3}$$

The density difference that makes up the integrand of Eq. (3) captures the relative buoyancy that a water parcel would experience as it moves from $z_r$ to $z$. Changes in density due to compressibility as the water parcel moves vertically are preserved in Eq. (3) and represented by pink shading in Fig. 1. In turn, gray shading in Fig. 1 represents the density difference between the parcel's density $\rho(\mathbf{x},t)$ at its actual position $\mathbf{x}$ and $\rho_r$. Given this, Tailleux (2018) defined precise conservation laws for $E_a$ and the local kinetic energy per unit mass ($E_k = \|\mathbf{u}\|^2/2$) of a fluid with the three-dimensional velocity ($\mathbf{u} = (u,v,w)$) as

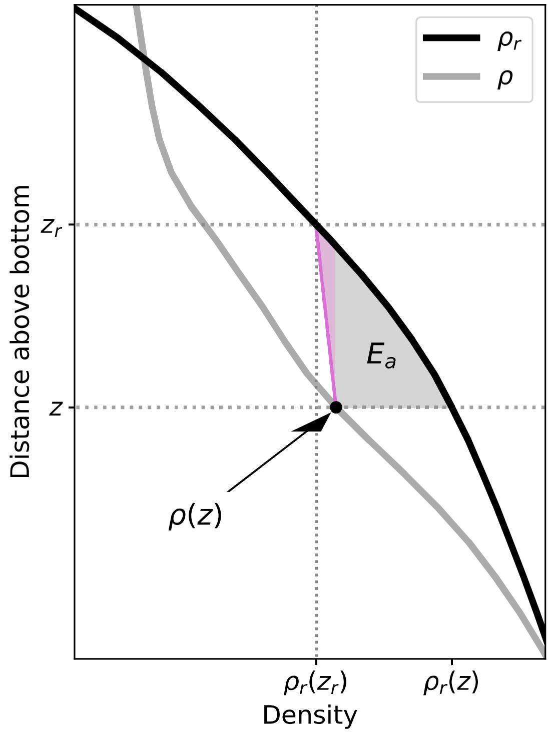


FIG. 1. Schematic explanation of $E_a$ as defined in Eq. (3). Given the in-situ density profile $\rho$ (gray line) and the fluid's $\rho_r$ (black line), $E_a$ evaluated at $z$ is proportional to the shaded area in gray and pink. Pink shading represents the effect of compressibility, as the diagonal pink line shows the change in $\rho$ due to adiabatic expansion of a water parcel that moves between pressure levels at $z$ and $z_r$.

$$\rho\frac{\partial}{\partial t}E_k = -\rho\mathbf{u}\cdot\nabla E_k - \mathbf{u}\cdot\nabla(p-p_r) - \rho' g w + \rho\mathbf{F}\cdot\mathbf{u} - \varepsilon, \tag{4}$$

and

$$\rho\frac{\partial E_a}{\partial t} = -\rho\mathbf{u}\cdot\nabla E_a + \rho' g w + \rho\dot{E}_a + \gamma, \tag{5}$$

where

$$\rho'(\mathbf{x},t) = \rho(\mathbf{x},t) - \rho_r(z,t). \tag{6}$$

Ordered as they appear, terms on the right hand side of Eq. (4) represent advection, pressure work, the rate of energy transfer from $E_k$ into $E_a$, viscous work ($\mathbf{F}$ represents viscous forces that include the wind stress), as well as dissipation and compressive terms that are grouped into $\varepsilon$ and will not be considered in calculations below given their relatively small magnitude. Similarly, terms in the right hand side of Eq. (5) represent advection, energy conversions from $E_k$, diabatic changes to $E_a$ (written as $\dot{E}_a$), and non-local effects ($\gamma$) that will not be further considered here.

Both the pressure work in Eq. (4) and the energy conversion term $\rho' g w$ depend on the choice of $\rho_r$. $p$ and $p_r$ are the hydrostatic pressures at $\mathbf{x}$ under the actual and the reference fluid states respectively. Similarly, conversions $\rho' g w$ between $E_k$ and $E_a$ are weighted by the perturbation density defined in Eq. (6).

### *a. Energy transfers between $E_k$ and $E_a$*

Notice that the term $\rho' g w$ appears with opposite signs in Eqs. (4) and (5), thus representing a transfer of energy between $E_k$ and $E_a$. When $\rho' g w > 0$, $E_k$ is used to move water parcels away from their $z_r$, much like when we stretch or compress a spring. In contrast, when $\rho' g w < 0$, energy stored in $E_a$ is released and transformed into $E_k$ whose motion brings water parcels closer to their respective $z_r$. We put particular focus on this term because it isolates $w$ and thus points to the energetic costs and implications of upwelling.

Energy transfers $\rho' g w$ in upwelling regions ($w > 0$) may flow in either direction between $E_k$ and $E_a$. This is profoundly consequential because it means that upwelling may be powered by either $E_k$ or $E_a$. Given the sign of $w$, the direction of local energy flows is thus determined by the sign of $\rho'$.

At locations $\mathbf{x}$ where $\rho' < 0$, upwelling can be powered by $E_a$ because the water parcel at $\mathbf{x}$ is located at a height lower than its reference level $z_r$, where $z$ is defined positive upwards. This means that buoyancy forces embedded in $\rho$ are already primed to push the water parcel upward and upwelling can occur without additional $E_k$ input. In such situations, we refer to the water parcel as 'light,' which is relative to both the parcel's $\rho$, its actual level $z$, and $\rho_r$. In contrast, when $\rho' > 0$, we refer to water parcels as 'heavy,' because they are located above their $z_r$ ($z > z_r$). Upward movement of such water parcels thus requires additional $E_k$ input that is transferred into the local $E_a$ at a rate $\rho' g w > 0$. On the flipside, downwelling ($w < 0$) of 'light' ($\rho' < 0$) water requires additional $E_k$ input, while $E_a$ powers the same motion for a 'heavy' ($\rho' > 0$) water parcel.

The dependence of energy flows on $\rho'$ and the choice of $\rho_r$ brings the concerning impression that deciding whether upwelling is powered by $E_a$ or $E_k$ is up to us and the methods used to compute $\rho_r$. However, careful interpretation of the balances between $\rho' g w$ and other terms in Eqs. (4)

and (5) ultimately lead to a detailed picture of the drivers and energetics of vertical motion that is self-consistent and whose sensitivity to the choice of $\rho_r$ is easily testable (Wong et al. 2016; Tailleux 2018).

The words 'light' and 'heavy' associated with the sign of $\rho'$ can make it seem like transfers between $E_k$ and $E_a$ must be associated with static instabilities. However, conversions of $E_a$ into $E_k$ described here can happen in a fluid that remains stably stratified everywhere (Turner 1969), and the vertical motions that concern us typically happen in concert with horizontal motions. Gravity currents and baroclinic instability help exemplify this particularly well; as lateral gradients drive high-$\rho$ parcels forward against low-$\rho$ ones, the low-$\rho$ parcels ascend and allow denser parcels to spread out across the bottom of the fluid volume. Thus, vertical motion emerges from lateral gradients in a fluid without requiring that the fluid is ever unstably stratified (Lorenz 1955).

### *b. Diabatic changes to $E_a$*

Reversible changes to $E_a$ occur through adiabatic rearrangements of water parcels that change $z$ and thus modify the displacement $(z - z_r)$. In contrast, irreversible changes $\dot{E}_a$ result from diabatic transformations of seawater properties $\Theta$ and $S$, which change a water parcel's $\rho$ and thus redefine its $z_r$ (Eq. 1). For example, a 'heavy' ($z > z_r$, $\rho' > 0$) water parcel can lose its $E_a$ when heat is added or $S$ removed diabatically to reduce $\rho$ and lift up $z_r$. Conversely, a 'light' ($z < z_r$, $\rho' < 0$) water parcel can lose its $E_a$ when its $\rho$ is diabatically increased and $z_r$ lowered. Following Tailleux (2013), we account for these effects in Eq. (5) through the term

$$\rho \dot{E}_a(\mathbf{x}, t) = g\left[\dot{\Theta} \int_{z_r}^{z} \frac{\partial \rho}{\partial \Theta} dz' + \dot{S} \int_{z_r}^{z} \frac{\partial \rho}{\partial S} dz'\right], \tag{7}$$

where the time derivatives $\dot{\Theta}$ and $\dot{S}$ are diabatic changes to $\Theta$ and $S$, respectively, which result from air-sea fluxes and ocean turbulence. Likewise, the integrands $\frac{\partial \rho}{\partial \Theta}$ and $\frac{\partial \rho}{\partial S}$ represent the rates of seawater contraction for changes in $\Theta$ and $S$.

### *c. Implementation on CESM2*

We used output from fully coupled historical simulations of CESM2 (Danabasoglu et al. 2020) to compute individual terms in Eqs. (4) and (5). A model, rather than a reanalysis product, is used here because the latter don't conserve energy. Furthermore, models allow precise estimation of terms in Eq. (7) as described below. Even though the numerics in CESM2 have many biases when compared to oceanographic observations, they are energetically and physically consistent. Thus, an ocean model can best help us leverage the precise conservation laws in Eqs. (5) and (4). To minimize the effects of transient eddies, all estimates shown below are computed from yearly-averaged quantities unless noted otherwise.

Some aspects of our results are sensitive to the choice of the fluid volume $V_r$, which sets $\rho_r$. $V_r$ was defined as the Pacific Ocean between 35°S and 35°N, corresponding roughly to the volume occupied by the STCs. We chose this area because our focus is on understanding energetic interactions between the ECS and STCs. More details on the sensitivity of our results to the choice of $V_r$ are given in the Discussion.

Given $V_r$, we computed time-dependent profiles of $\rho_r$ by rearranging water parcels across $V_r$ for both monthly- and yearly-averaged output. To do so, we binned the surface potential density $\sigma_0$ in 0.125 kg m$^{-3}$ increments for all grid cells across $V_r$. We then estimated the total volume of seawater in each density class and allocated water masses to different reference depths $z_r$ while constraining the amount of volume available at each level. Numerically, this was achieved by relating cumulative density functions of $\sigma_0$ and of the distribution of volume available for seawater storage across $V_r$ as a function of $z_r$. Once sorted, we used a linear compressibility coefficient to approximate the effect of pressure as parcels were converted from $\sigma_0$ back into $\rho$. This method is roughly equivalent to the surface-to-bottom, volume-frequency approach tested in Saenz et al. (2015), with the exception that our approach is based on $\sigma_0$ and does not preserve the full distinct effects of $\Theta$ and $S$ on $\rho_r$.

The diabatic term $\rho \dot{E}_a$ was computed using Eq. (7) with $\dot{\Theta} = \frac{\partial \Theta}{\partial t} + \mathbf{u} \cdot \nabla \Theta$ and $\dot{S} = \frac{\partial S}{\partial t} + \mathbf{u} \cdot \nabla S$ computed as the sum of Eulerian and advective time tendencies of temperature and salinity respectively. CESM2 outputs time-averaged values of these tendencies under variable names TEND-TEMP, TEND-SALT, TOT-ADV-TEMP, and TOT-ADV-SALT. Seawater properties including the dependence of $\sigma_0$ on $\Theta$ and $S$, linear compressibility coefficients, and integrands in Eq. (7) were computed using the Gibbs SeaWater Toolbox (McDougall and Barker 2011).

## 3. Results

The tilt of the equatorial thermocline produces a zonal contrast in $\rho'$, with light ($\rho' < 0$) water in the west and heavy ($\rho' > 0$) water in the east (Fig. 2). Values of $z - z_r$ indicate that, without additional energy inputs, water parcels in the western Pacific thermocline can move upward by as much as 60 m. Similarly, the eastern Pacific thermocline has the $E_a$ necessary to move downwards by as much as 90 m (Figs. 2c,d). As we show below, equatorial upwelling in regions where $z - z_r < 0$ ($\rho' < 0$) is powered by $E_a$, implying that those waters cannot be lifted directly by winds along the equator.

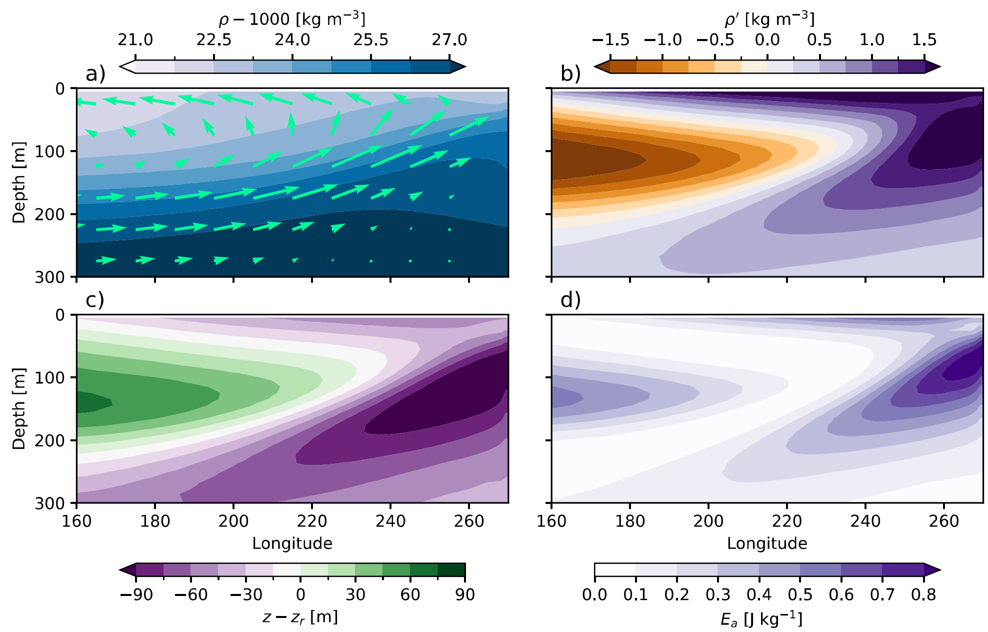


FIG. 2. Mean state of potential energy in the equatorial Pacific (3°S, 3°N). Color shading shows a) $\rho$, b) $\rho'$, c) $z - z_r$, and d) $E_a$, while the arrows in a) show the mean velocities $(u, w)$ with $w$ magnified for clarity.

Equatorial upwelling is powered by both $E_k$ and $E_a$. The zonal tilt in the equatorial thermocline makes it such that 'light' water with $\rho' < 0$ covers much of the Western and Central equatorial Pacific thermocline. Therefore, water masses here move closer to their $z_r$ as they move up and eastward along the Equatorial Undercurrent (EUC). This results in $\rho' g w < 0$ and implies a transfer from $E_a$ into $E_k$ (blue shading in Fig. 3a). In contrast, 'heavy' water in the Eastern Pacific uses up $E_k$ and converts it into $E_a$ (red shading in Fig. 3a). Closing the energetic balance of equatorial upwelling thus requires that we find sources of $E_a$ in the west but sources of $E_k$ in the east. In areas where $\rho' g w > 0$, we may point to the wind stress $\mathbf{F}$ as the energy source that explains upwelling (Eq. 4). However, $\mathbf{F}$ does not appear in Eq. (5) and cannot directly explain upwelling in regions where $\rho' g w < 0$.

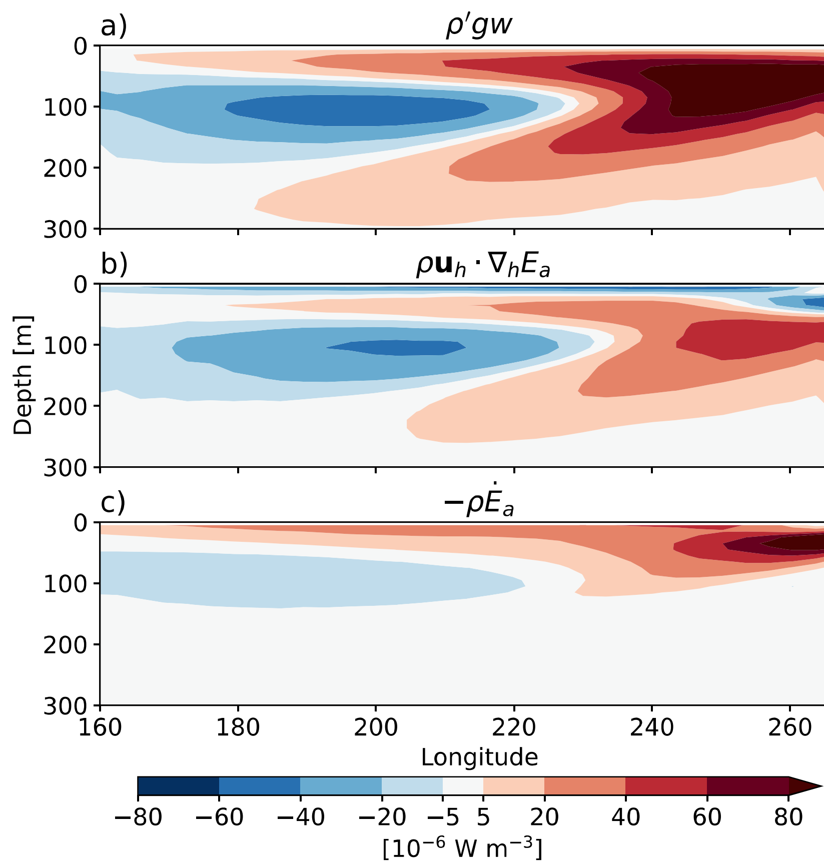


FIG. 3. Energetic balance of equatorial upwelling. Temporal averages of a) $\rho' g w$, b) $\rho \mathbf{u}_h \cdot \nabla_h E_a$, and c) $-\rho \dot{E}_a$ using yearly output from a historical CESM2 run. All values are averaged between 3°S and 3°N. The thermocline follows the approximate balance $\rho' g w \approx \rho \mathbf{u}_h \cdot \nabla_h E_a - \rho \dot{E}_a$.

Horizontal advection of $E_a$ into the Western and Central Pacific thermocline supplies most of the energy necessary to drive upwelling there (Fig. 3b). Inspection of all three-dimensional components of $E_a$ convergence (Fig. S1) suggests that meridional advection makes the greatest contribution to the balance $\rho' g w$, while diabatic processes $-\rho \dot{E}_a$ supply additional $E_a$ at shallower levels (Fig. 3c). Altogether, the sum $\rho \mathbf{u}_h \cdot \nabla_h E_a - \rho \dot{E}_a$ continuously supplies the $E_a$ necessary to lift water parcels in the Western Pacific thermocline vertically by $\sim 40$ m, where the subscript $h$

implies that only the horizontal components of $\mathbf{u}$ and $\nabla E_a$ are being considered. This supports the view in Kleeman et al. (1999) that equatorial upwelling can be pushed from below.

### *a. Sources of $E_a$*

Let us now turn our attention to Eq. (5) in search of sources of $E_a$ and mechanisms that may transport energy into areas where $\rho' g w < 0$ (Fig. 3a). Sources of $E_a$ exist wherever the absolute difference $\|z - z_r\|$ of a given water parcel increases over time. Namely, wherever

- 'heavy' ($\rho' > 0$) water moves upward ($w > 0$),
- 'light' ($\rho' < 0$) water moves downward ($w < 0$),
- diabatic changes to temperature or salinity quantified by $\dot{\Theta}$ and $\dot{S}$ move a water parcel's $z_r$ farther away from its actual position $z$.

Notice, that reversible changes in $E_a$ that are captured by $\rho' g w$ don't necessarily imply a local net source of ocean energy. Therefore, we refer to 'production' and 'usage' of $E_a$ to describe instances of reversible energy transfer that result from vertical motion.

Vertical integrals of $\rho' g w$ across the STCs (Fig. 4) highlight areas where $E_a$ is produced (red shading) and used (blue shading). Likewise, diabatic contributions $\rho \dot{E}_a$ are shown in Fig. 5. Most importantly, we find that downwelling branches of the near-equatorial overturning cells are the primary supplier of western equatorial thermocline $E_a$ (Fig. 4a). Wind-driven downwelling of 'light' waters in these regions creates two reservoirs of $E_a$ that flank the equator around 5°S and 5°N, and that flow towards it (Figs. 6, 4a). $E_a$ that flows equatorward from off-equatorial downwelling regions is used to drive upwelling along the EUC and thus transformed back into $E_k$ (Fig. 4b).

When flowing up eastward along the EUC, water parcels eventually reach their own $z_r$ and thus exhaust their $E_a$. $z_r$, however, does not remain static as vertical and lateral mixing induce diabatic warming ($\dot{\Theta} > 0$) such that $z_r$ is gradually lifted for western equatorial subsurface waters (Figs. 3c). The majority of this warming is caused by parameterized eddy stirring between the equatorial thermocline and the warmer near-equatorial downwelling cells (Fig. 5b). After water parcels reach their $z_r$ flowing along the EUC, their continued ascent becomes powered by $E_k$, so that they gain $E_a$ once more (Fig. 4c). Two processes balance this gradual increase in $E_a$ by upwelling water

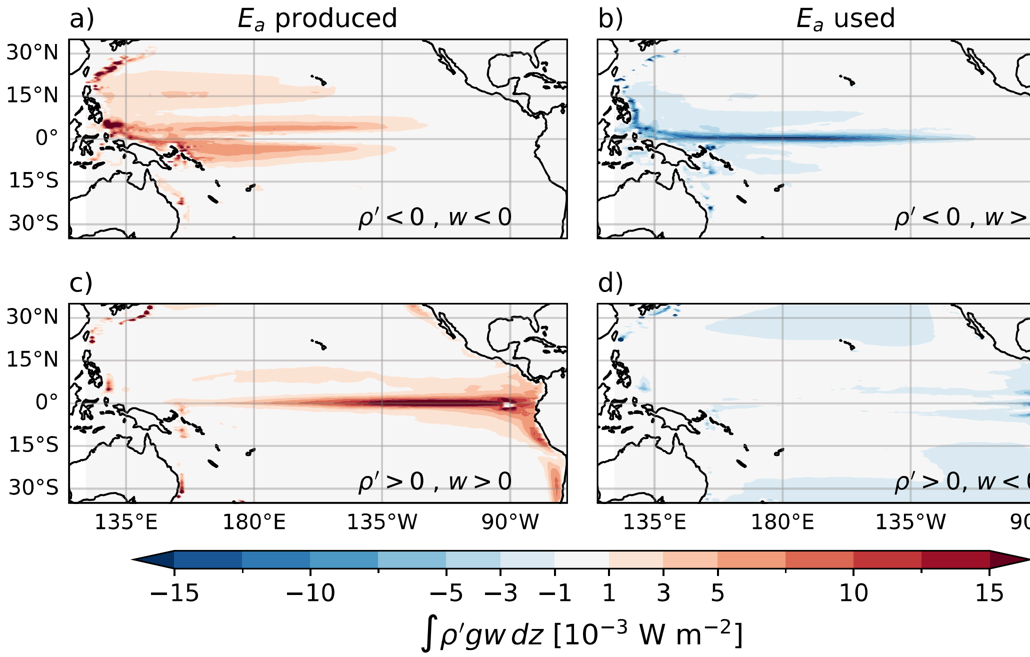


FIG. 4. Vertical integrals $\int \rho' g w \, dz$ reveal $E_k \rightarrow E_a$ energy transfers, divided into processes that (left) produce and (right) use $E_a$. Red shading in a) and c) indicates production of $E_a$, while blue shading in b) and d) indicates that $E_a$ is being used to produce $E_k$.

parcels in the eastern Pacific. First, $E_a$-poor waters are advected eastward along the EUC into the eastern equatorial thermocline where $\rho \mathbf{u}_h \cdot \nabla h E_a > 0$ and $z > z_r$; this enables a steady state in $E_a$ despite persistent $\rho' g w > 0$ (Figs. 2c,d, 3a,b). Second, diabatic heating of 'heavy' near-surface water in the cold tongue region lowers the density of water parcels and thus lifts their $z_r$, ultimately lowering $E_a$ (Fig. 5a).

$E_a$-driven upwelling would be impossible without diabatic heating of near-surface waters in the cold tongue (Fig. 5a). Diabatically lifting the $z_r$ of water parcels towards the surface ensures that $E_a$ is produced when those water parcels enter downwelling regions. If water parcels preserved their density as they flow out of the cold tongue, they would still have $\rho' \sim 1$ kg m$^{-3}$ when they reached downwelling regions and would readily move downwards by using $E_a$ rather than producing it. Thus, a near-equatorial energy cycle emerges:

1. $E_a$ is used by central Pacific upwelling and transferred into $E_k$ (regions where $\rho' g w < 0$ in Figs. 3a, 4b)

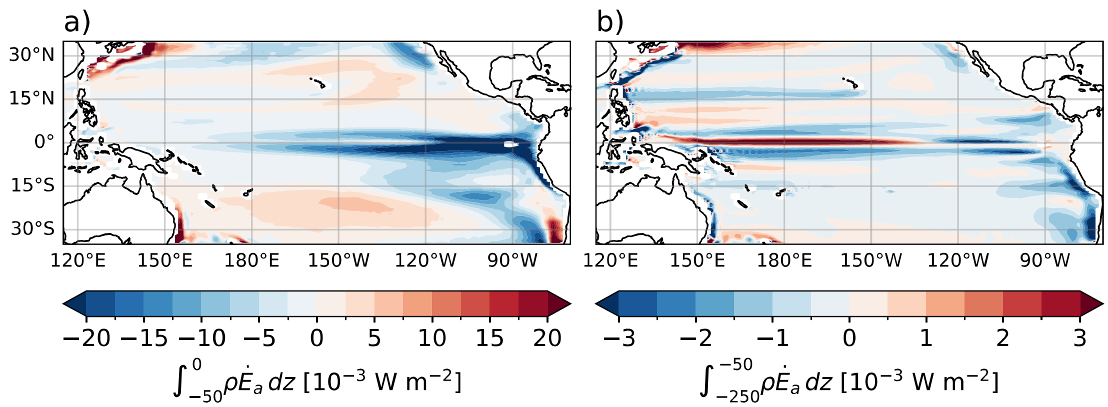


Fig. 5. Diabatic sources and sinks of $E_a$, integrated over a) the top 50 meters, and b) between 50 and 300 meters depth.

2. $E_k$ is used to drive upwelling in the eastern equatorial Pacific. This increases the $E_a$ of 'heavy' ($\rho' > 0$) water parcels that reach the surface cold tongue (Figs. 2b, 3a, 4c).

3. Diabatic heating reduces the density of surface waters as they flow out of the cold tongue, thus lifting their $z_r$, reducing their $E_a$, and anchoring water parcels to the surface (Fig. 3c, 5a)

4. Near-equatorial winds supply $E_k$ to drive downwelling in the near-equatorial cells and create $E_a$ reservoirs that flank the equator (Figs. 4a, 6a).

5. Recently-downwelled waters carrying excess $E_a$ flow towards the equator and supply the energy necessary to drive upwelling in the central Pacific thermocline (Figs. 3b), thus restarting the cycle.

Additional thermocline reservoirs of $E_a$ exist poleward of 10°S and 10°N (Fig. 6a). Thermocline energy storage is more prominent in the northwestern Pacific, where $E_a$ is produced via downwelling of 'light' water in the subtropical gyre south of 25°N (Fig. 4a). At higher latitudes, downwelling in the gyre happens for water with $\rho' > 0$ and thus uses near-surface $E_a$ to produce $E_k$ (Figs. 4d). Continuous transfers between $E_a$ and $E_k$ also take place in the southeastern Pacific, where coastal upwelling lifts heavy water to produce $E_a$ off the Peruvian coast (Fig. 4c). The energetics here, however, are fundamentally different to those in the cold tongue, since $\rho \dot{E}_a > 0$ helps water parcels sink and release $E_k$ (Figs. 5a, 4d) rather than anchor them to the surface. Moreover, the sign

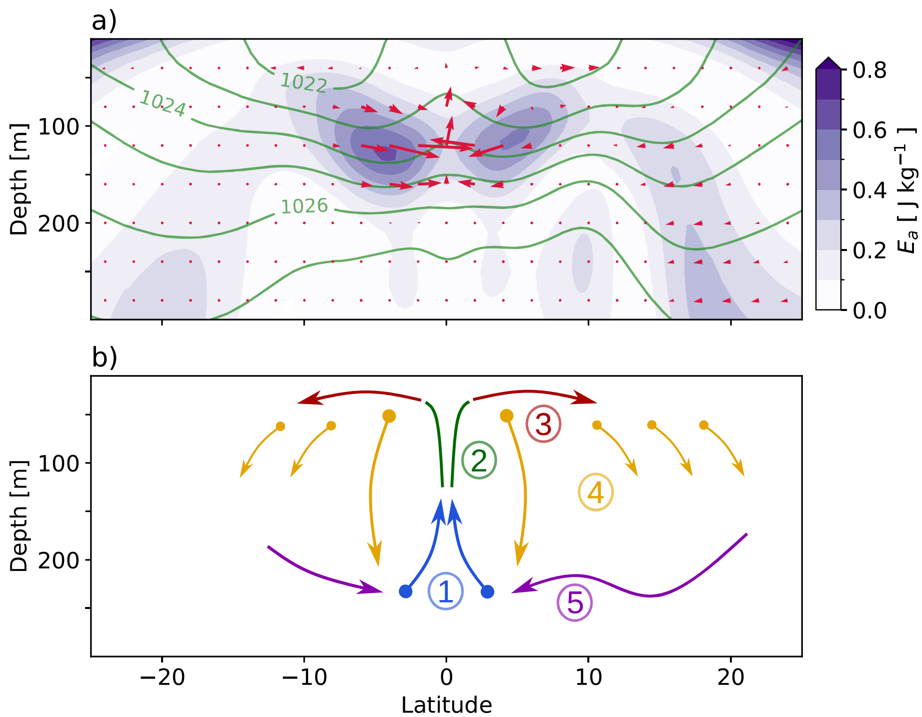


FIG. 6. Meridional view of $E_a$ storage and transport in the western-to-central Pacific ocean (values averaged between 160°E and 220°E). Color shading shows a) $E_a$ and its transport $\mathbf{u}E_a$ (red arrows), with the vertical component exaggerated for clarity. Green contours show isopycnals at 1 kg m$^{-3}$ intervals. b) schematic representation of the energy cycle described in Section 3.1. Color-coded arrows and numbers refer to each step in that cycle.

$\rho \dot{E}_a > 0$ directly off the Peruvian coast is determined by $\dot{\Theta} < 0$ that results from parameterized eddy stirring rather than surface heat fluxes.

Equatorward flows connect the northwest Pacific $E_a$ reservoir to the equatorial cell (Fig. 6a). This implies the possibility that subtropical regions help regulate equatorial upwelling, as momentum and buoyancy forcing in the subtropical gyre will determine the rate of $E_a$ transport into the equatorial region (Figs. 4a). Notice, however, that the region pictured in Fig. 6 does not include the Mindanao western boundary current, which mediates additional transport from the north Pacific subtropical gyre to the equatorial region. A complete isolation of near-equatorial and subtropical routes of equatorward $E_a$ transport is beyond the scope of this study. Still, we point out that the western boundary contribution to $E_a$-driven equatorial upwelling may be better captured by the zonal advective component $\rho u \frac{\partial E_a}{\partial x}$ in the western end of the EUC (Fig. S1).

*b. Temporal variability and relation to cold tongue upwelling*

Thermocline-driven upwelling is primarily powered by the trade winds via near-equatorial downwelling of warm waters (Fig. 4a). Thus, thermocline storage and advection of $E_a$ can help us study forms of equatorial variability that are related to the trade winds. Previous studies by Brown and Fedorov (2008, 2010); Brown et al. (2011) have shown that El Niño-Southern Oscillation (ENSO) can be represented as a cycle between trade wind strength and the zonally-integrated equatorial $E_a$. Here, we take advantage of the precise conservation laws in Eqs. (4) and (5) to bring a new perspective to the oceanic role in ENSO cycles. To do so, we computed the El Niño 3.4 index from our CESM2 runs and used monthly-averaged model output to create average composites of the equatorial energy balance under El Niño and La Niña conditions (Fig. 7).

As noted by Brown and Fedorov (2008), $E_a$ storage in the equatorial Pacific is intimately tied to the zonal thermocline tilt (Figs. 2a,d). This tilt implies that water parcels in the west can upwell without additional energy input ($z - z_r > 0$) while parcels in the east could readily downwell ($z - z_r < 0$, Fig. 2c). The tilted thermocline and $E_a$ pattern it implies are sustained by $E_k$ input by winds, but the conversion from $E_k$ to $E_a$ is mediated by off-equatorial downwelling in the west (Fig. 4a), while the conversion from $E_k$ to $E_a$ may happen directly via Ekman-style upwelling in the east (Fig. 4c).

When the winds weaken during El Niño events, $E_a$ production falls across the near-equatorial region. As a result, $\rho \mathbf{u}_h \cdot \nabla_h E_a$ weakens in the western equatorial thermocline and a fraction of the potential vertical displacements stored in $E_a$ becomes realized (Fig. 7a,b). A decrease in thermocline tilt is possible because $E_a$ stored in each end of the basin can be used to drive upwelling in the west and downwelling in the east (Fig. 2c). As $E_a$ is used by vertical motions and off-equatorial $E_a$ production is weakened, equatorial $E_a$ is depleted and buoyancy forces reach a new balance. The low-$E_a$ state that characterizes El Niño events is directly opposite to the mechanisms that unfold during La Niña. When the trade winds strengthen, $E_a$ production associated with both equatorial upwelling (Fig. 4c) and off-equatorial downwelling (Fig. 4a) is increased. As a result, the thermocline tilt strengthens and equatorial $E_a$ storage grows (Fig. 7c,d).

Changes in $E_a$ and $\rho \mathbf{u}_h \cdot \nabla_h E_a$ across ENSO cycles are consistent with changes in upwelling that are crucial to ENSO theory (Fig. 7). This shows that $E_a$-driven upwelling is crucial not only to the mean state, but can also help understand equatorial variability. While thermocline-driven

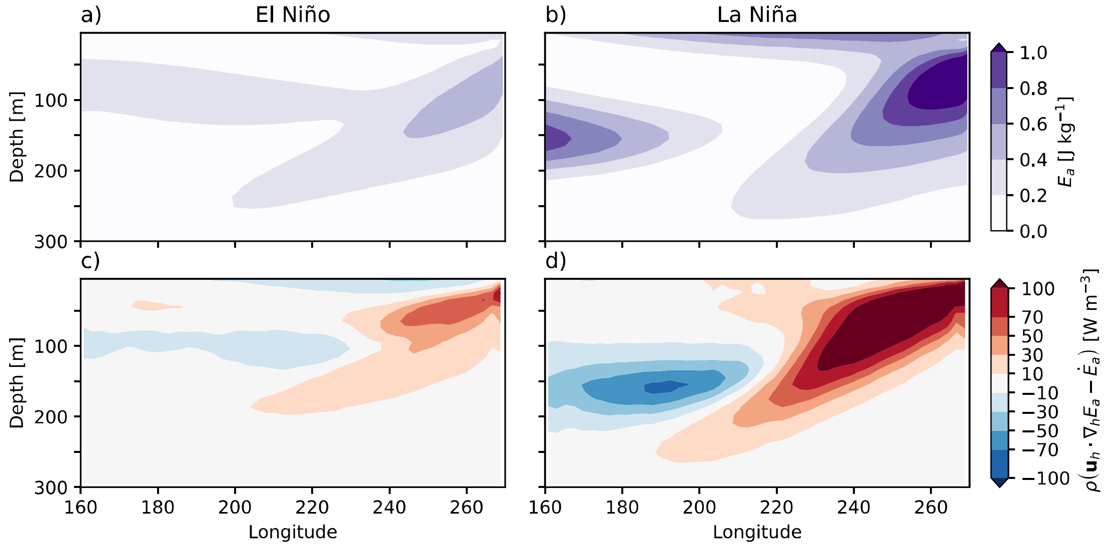


FIG. 7. Equatorial balance of $E_a$ during El Niño (left column) and La Niña (right column). Color shading in a) and b) shows $E_a$, while shading in c) and d) shows $\rho \mathbf{u}_h \cdot \nabla_h E_a - \rho \dot{E}_a$, which is the sum of terms in Figs. 3b,c.

upwelling happens in the western and central equatorial Pacific, its upward push initiates the ascent of water parcels that flow eastward along the EUC. As a result, conversion of $E_a$ into $E_k$ via thermocline upwelling helps shape subsurface conditions in the cold tongue region.

### *c. Sensitivity to $V_r$ and $\rho_r$*

Estimates shown above use reference profiles $\rho_r(z,t)$ that were obtained by adiabatically rearranging Pacific Ocean water parcels between 35°S and 35°N. Changing the reference volume $V_r$ within which mass is rearranged impacts quantitative aspects of our results, but it doesn't change the fact that 'light' water spans the western equatorial Pacific thermocline. As we expand $V_r$ to higher latitudes, $V_r$ includes more high-density water masses and an increasing fraction of the equatorial Pacific thermocline is perceived as 'light' ($\rho' < 0$). As a result, expanding $V_r$ increases the fraction of equatorial upwelling that is powered by $E_a$ (Fig. 8).

To test the sensitivity of our results and find a feasible range for the values of energy transfers, we defined instances of $V_r$ that extend across the Pacific, between limit latitudes ($\phi$°S,$\phi$° N), and down to 800 m depth. Given the profiles $\rho_r$ that resulted from each choice of $V_r$, we estimated the two indicators in Eqs. (8) and (9) to evaluate the energetic cost of upwelling and the role of $E_a$ under all conditions (Fig. 8).

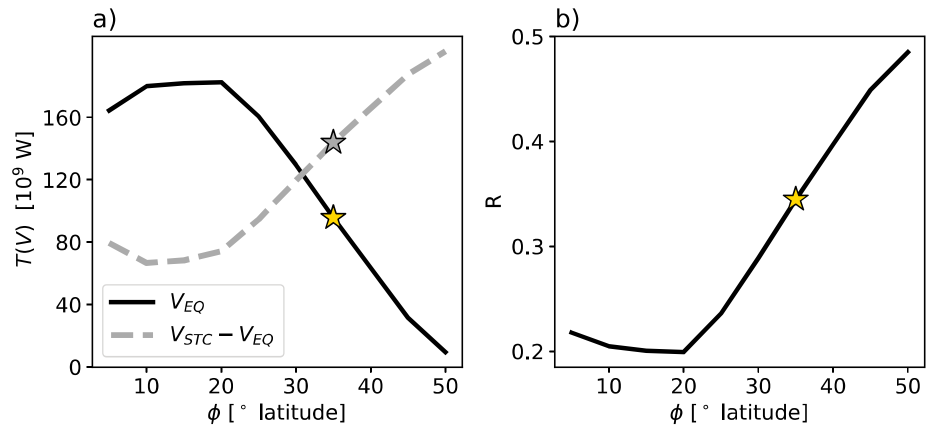


FIG. 8. Sensitivity of energy transfers to the latitudinal extent of $V_r$. a) the total $E_k$ input needed to sustain vertical motions in the near-equatorial region ($V_{EQ}$, between 3°S and 3°N), and in the rest of the STCs ($V_{STC} - V_{EQ}$, from 35°S to 35°N excluding $V_{EQ}$). Stars indicate the value $\phi = 35°$ used to produce all other figures in this study.

$T(V)$ is the total $E_k$ input necessary to sustain vertical motions within a volume $V$ (Eq. 8), and serves as a proxy for the local wind contribution to driving vertical motions within $V$. Estimates for the Pacific equatorial region $V_{EQ}$ (between 3°S and 3°N), and the STC region $V_{STC} - V_{EQ}$ (between 35°S and 35°N excluding $V_{EQ}$) are shown in Fig. 8a. Similarly, $R$ is defined for $V_{EQ}$ as the fraction of reversible energy transfers $\rho' g w$ between $E_k$ and $E_a$ that must be balanced by sources of $E_a$. The denominator in Eq. (9) uses the Heaviside function $H(-\rho' g w)$ to only account for areas where $E_a$ is transformed into $E_k$.

$$T(V) = \int_V \rho' g w \, dV \tag{8}$$

$$R = \int_{V_{EQ}} |\rho' g w| H(-\rho' g w) \, dV \Big/ \int_{V_{EQ}} |\rho' g w| \, dV \tag{9}$$

As $V_r$ extends beyond the tropical Pacific, sustaining vertical motions in $V_{EQ}$ takes up more $E_a$ and requires a lower $E_k$ input. The decrease in $T(V_{EQ})$ is mirrored by increases in $T(V_{STC} - V_{EQ})$ (Fig. 8a). Correspondence between $T(V_{EQ})$ and $T(V_{STC} - V_{EQ})$ implies that $E_a$ used to power upwelling in $V_{EQ}$ is sourced from off-equatorial regions (Fig. 4a). As $V_r$ extends beyond the tropics, $E_a$ production by wind-driven downwelling increases because the subsurface tropical ocean is more likely to have $\rho' < 0$. Thus, expanding $V_r$ to higher latitudes helps to better account for the energy spent heating the tropical thermocline. As the energetics of subsurface heating become accounted for, powering equatorial upwelling increasingly becomes a matter of charging the tropical thermocline with $E_a$ and less a matter of supplying $E_k$ directly to the Equator (Fig. 8b).

Based on the sensitivity analysis in Fig. 8b, we assess that 20-50% of energy used by equatorial upwelling must be powered by $E_a$. This is a lower bound for the thermocline's energetic contribution to equatorial upwelling, since the thermocline could also supply $E_k$ to some equatorial regions where $\rho' g w > 0$ (Fig. 3a). Our analyses point to the importance of energy exchanges between equatorial and off-equatorial regions (Fig. 6, 8a) via the near-equatorial cells and the STCs alike. Based on these results and the fact that the STCs supply the water masses that upwell along the EUC (Lu et al. 1998; Nie et al. 2019), we chose $V_r$ to span the Pacific from 35°S to 35°N and speculate that the thermocline's energetic contribution to equatorial upwelling is closer to 50% than it is to 20%.

## 4. Discussion

The notion that equatorial upwelling is partly 'pushed from below' may be surprising at first. However, it follows straightforwardly from the production of $E_a$ by off-equatorial, wind-driven downwelling (Fig. 4a). As warm, low-density surface waters move down into the thermocline, they acquire $\rho' < 0$ and help sustain buoyancy forces that push water upward. Therefore, our analysis does not negate Wyrtki (1981), but simply highlights the storage of thermocline $E_a$ as a necessary intermediate step between Pacific wind forcing and equatorial upwelling. It is likely that the thermocline also drives upwelling by supplying $E_k$ to areas where $\rho' g w > 0$; for example, those below 200 m depth in Fig. 3a, which is far beyond the direct reach of wind stress. However, a thorough analysis of the $E_k$ balance is beyond the scope of this study.

Quantifying the energetic contribution of thermocline buoyancy forces to equatorial upwelling helps clarify connections between the ECS and the STCs (Figs. 6, 8). Transfer of $E_a$ from the STCs to the equator happens via mid-ocean equatorward flows (Fig. 6) and western boundary currents alike. The constant supply of $E_a$ from off-equatorial sources ensures that water parcels in the western equatorial Pacific thermocline are able to upwell without additional energy inputs (Fig.

2c). When this supply weakens or strengthens during ENSO cycles, the equatorial thermocline releases or takes up more $E_a$ and adjusts its tilt to match the changing conditions (Figs. 7).

Dynamical theories of equatorial upwelling have historically relied on mass balances to understand vertical motions (Wyrtki 1981; Kleeman et al. 1999). In that sense, theories have focused on ensuring consistency between horizontal forces and vertical velocities, rather than directly explaining the latter. The energetics framework described here may help formalize existing theories of equatorial upwelling, of its variability, and its connections to remote ocean conditions. Ultimately, evaluating the diversity of modeled equatorial Pacific responses to climate change requires that we find more satisfying explanations of upwelling velocities and that we learn to disentangle those from the thermodynamical implications of upwelling.

An important takeaway from our study is that thermal anomalies advected equatorward are not passive tracers, as is often assumed (Gu and Philander 1997). Rather, thermal anomalies across the STC can shape upwelling dynamics by changing the $z_r$ and $E_a$ of water parcels entering the equatorial region. More intuitively, think that it takes more energy to lift cold, high-density water than it takes to lift warm water with low density. This is true for the energetics of upwelling that is powered by either $E_a$ or $E_k$. Future studies may use idealized modeling to test the extent to which density changes impact equatorial $w$ under a fixed wind stress.

Previous studies had analyzed the equatorial Pacific ocean from an available energetics perspective across multiple timescales (Fedorov 2002; Brown and Fedorov 2008, 2010; Brown et al. 2011; Shi et al. 2020). By adopting the more precise framework of available energetics formulated by Tailleux (2013, 2018), we are able to trace the sources of $E_a$ that keep the equatorial thermocline tilted with upwelling along the EUC. This way, we find that $E_a$ stored in the equatorial mean state (Fig. 2d) does not sit passively. Instead, our analysis shows that this $E_a$ is actively used to power upwelling and replenished by low-density equatorward thermocline flows in the western-to-central Pacific (Fig. 6). These realizations were only possible because we used a framework of local available energetics with local conservation laws (Tailleux 2013, 2018), whereas previous studies had used basin-integrated measures of available energy.

Our results suggest that downwelling in the near-equatorial cells may be just as important to equatorial upwelling as upwelling itself. Scarce measurements exist in this off-equatorial region, and non-linear interactions between the mean circulation and tropical instability waves make for a complicated physical picture (Perez and Kessler 2009). A fraction of this effect may be captured by the diabatic term $\rho\dot{E}_a$ (Figs. 3c, 5b), which suggests that vertical and lateral mixing supply a non-negligible fraction of all the $E_a$ used to power equatorial upwelling. Still, further work is needed to clarify how precise knowledge of off-equatorial downwelling and tropical instability waves may help better understand upwelling as well as broader modes of Pacific variability.

## 5. Conclusion

We used the Boussinesq local available energetics framework of Tailleux (2013, 2018) to detail the tropical thermocline's role in driving equatorial upwelling. Our analysis show that at least 20-50% of the energy involved in equatorial upwellling is supplied by the off-equatorial thermocline (Fig. 8b). This result follows from the low $\rho$ of the western Pacific thermocline, which implies $\rho' < 0$ and thus allows 20-50% of the energy spent on equatorial upwelling to be supplied by $E_a$ rather than $E_k$ (Figs. 2, 3, 8). This implies that equatorial upwelling is partly pushed from below, and not only pulled from above, as intuition and mass balance arguments may suggest Wyrtki (1981). This remote influence from below may help explain why equatorial upwelling has been observed in the presence of local westerly winds (Helber and Weisberg 2001).

We find evidence of a near-equatorial cycle involving vertical motions driven by both $E_a$ and $E_k$, as well as diabatic changes to $E_a$ caused by surface heating in the cold tongue (Fig. 6b). Reversible energy transfers that arise from vertical motions respond to variations in the trade winds and are thus in general agreement with classical theories of equatorial variability (Fig. 7). Our findings differ from common understanding, however, in that they establish a link between upwelling velocities and surface buoyancy fluxes. This link exists primarily because off-equatorial downwelling would not charge the thermocline with $E_a$ if water parcels flowing out of the cold tongue preserved their $\rho$ (Figs. 4a, 5a).

Lastly, we reiterate how our analyses point to near-equatorial downwelling as a crucial process helping control equatorial upwelling. Even though schematic depictions of the near-equatorial cells hint at a meaningful connection between equatorial and off-equatorial vertical motions (Lu et al. 1998), those links have lacked a dynamical basis beyond mass conservation. The analyses of local available energetics presented here may help better leverage connections between vertical motions across the tropical oceans in studies of global climate dynamics.

*Acknowledgments.* Without implying their endorsement, the authors are grateful for fruitful discussions with Rémi Tailleux, Feng Jiang, and Mark Cane. This work was funded by grant DE SC-0023333 from the US Department of Energy and grants AGS 22-17618 and OCE-2219829 from the National Science Foundation.

*Data availability statement.* Data and code used to produce the figures in this manuscript can be found in zenodo.org/records/13741896.

This shows how to enter the commands for making a bibliography using BibTeX. It uses references.bib and the ametsocV6.bst file for the style.

## References

Brown, J. N., and A. V. Fedorov, 2008: Mean energy balance in the tropical pacific ocean. *Journal of Marine Research*, **66 (1)**, 1–23.

Brown, J. N., and A. V. Fedorov, 2010: How much energy is transferred from the winds to the thermocline on enso time scales? *Journal of Climate*, **23 (6)**, 1563–1580, https://doi.org/doi.org/10.1175/2009JCLI2914.1.

Brown, J. N., A. V. Fedorov, and E. Guilyardi, 2011: How well do coupled models replicate ocean energetics relevant to enso? *Climate Dynamics*, **36**, 2147–2158, https://doi.org/doi.org/10.1007/s00382-010-0926-8.

Capotondi, A., and Coauthors, 2023: Mechanisms of tropical pacific decadal variability. *Nature Reviews Earth & Environment*, **4 (11)**, 754–769, https://doi.org/doi.org/10.1038/s43017-023-00486-x.

Clement, A. C., R. Seager, M. A. Cane, and S. E. Zebiak, 1996: An ocean dynamical thermostat. *Journal of Climate*, **9 (9)**, 2190–2196, https://doi.org/doi.org/10.1175/1520-0442(1996)009⟨2190:AODT⟩2.0.CO;2.

Coats, S., and K. Karnauskas, 2017: Are simulated and observed twentieth century tropical pacific sea surface temperature trends significant relative to internal variability? *Geophysical Research Letters*, **44 (19)**, 9928–9937, https://doi.org/doi.org/10.1002/2017GL074622.

Danabasoglu, G., and Coauthors, 2020: The community earth system model version 2 (cesm2). *Journal of Advances in Modeling Earth Systems*, **12 (2)**, e2019MS001 916, https://doi.org/doi.org/10.1029/2019MS001916.

Fedorov, A. V., 2002: The response of the coupled tropical ocean–atmosphere to westerly wind bursts. *Quarterly Journal of the Royal Meteorological Society: A journal of the atmospheric sciences, applied meteorology and physical oceanography*, **128 (579)**, 1–23, https://doi.org/doi.org/10.1002/qj.200212857901.

Gu, D., and S. G. Philander, 1997: Interdecadal climate fluctuations that depend on exchanges between the tropics and extratropics. *Science*, **275 (5301)**, 805–807, https://doi.org/doi.org/10.1126/science.275.5301.805.

Heede, U. K., and A. V. Fedorov, 2021: Eastern equatorial pacific warming delayed by aerosols and thermostat response to co2 increase. *Nature Climate Change*, **11 (8)**, 696–703, https://doi.org/doi.org/10.1038/s41558-021-01101-x.

Heede, U. K., and A. V. Fedorov, 2023: Colder eastern equatorial pacific and stronger walker circulation in the early 21st century: Separating the forced response to global warming from natural variability. *Geophysical Research Letters*, **50 (3)**, e2022GL101 020, https://doi.org/doi.org/10.1029/2022GL101020.

Helber, R. W., and R. H. Weisberg, 2001: Equatorial upwelling in the western pacific warm pool. *Journal of Geophysical Research: Oceans*, **106 (C5)**, 8989–9003, https://doi.org/doi.org/10.1029/2000JC000401.

Holliday, D., and M. E. Mcintyre, 1981: On potential energy density in an incompressible, stratified fluid. *Journal of Fluid Mechanics*, **107**, 221–225, https://doi.org/doi.org/10.1017/S0022112081001742.

Huang, R. X., 1998: Mixing and available potential energy in a boussinesq ocean. *Journal of Physical Oceanography*, **28 (4)**, 669–678, https://doi.org/doi.org/10.1175/1520-0485(1998)028⟨0669:MAAPEI⟩2.0.CO;2.

Hwang, Y.-T., S.-P. Xie, P.-J. Chen, H.-Y. Tseng, and C. Deser, 2024: Contribution of anthropogenic aerosols to persistent la niña-like conditions in the early 21st century. *Proceedings of the National Academy of Sciences*, **121 (5)**, e2315124 121, https://doi.org/doi.org/10.1073/pnas.2315124121.

Kang, D., and O. Fringer, 2010: On the calculation of available potential energy in internal wave fields. *Journal of Physical Oceanography*, **40 (11)**, 2539–2545, https://doi.org/doi.org/10.1175/2010JPO4497.1.

Kang, S. M., P. Ceppi, Y. Yu, and I.-S. Kang, 2023: Recent global climate feedback controlled by southern ocean cooling. *Nature Geoscience*, **16 (9)**, 775–780, https://doi.org/doi.org/10.1038/s41561-023-01256-6.

Karnauskas, K. B., R. Seager, A. Kaplan, Y. Kushnir, and M. A. Cane, 2009: Observed strengthening of the zonal sea surface temperature gradient across the equatorial pacific ocean. *Journal of Climate*, **22 (16)**, 4316–4321, https://doi.org/doi.org/10.1175/2009JCLI2936.1.

Kleeman, R., J. P. McCreary Jr, and B. A. Klinger, 1999: A mechanism for generating enso decadal variability. *Geophysical Research Letters*, **26 (12)**, 1743–1746, https://doi.org/doi.org/10.1029/1999GL900352.

Knutson, T. R., and S. Manabe, 1995: Time-mean response over the tropical pacific to increased c02 in a coupled ocean-atmosphere model. *Journal of Climate*, **8 (9)**, 2181–2199, https://doi.org/doi.org/10.1175/1520-0442(1995)008⟨2181:TMROTT⟩2.0.CO;2.

Lorenz, E. N., 1955: Available potential energy and the maintenance of the general circulation. *Tellus*, **7 (2)**, 157–167, https://doi.org/doi.org/10.3402/tellusa.v7i2.8796.

Lu, P., J. P. McCreary Jr, and B. A. Klinger, 1998: Meridional circulation cells and the source waters of the pacific equatorial undercurrent. *Journal of Physical Oceanography*, **28 (1)**, 62–84, https://doi.org/doi.org/10.1175/1520-0485(1998)028⟨0062:MCCATS⟩2.0.CO;2.

Luo, J.-J., S. Masson, S. Behera, P. Delecluse, S. Gualdi, A. Navarra, and T. Yamagata, 2003: South pacific origin of the decadal enso-like variation as simulated by a coupled gcm. *Geophysical Research Letters*, **30 (24)**, https://doi.org/doi.org/10.1029/2003GL018649.

McDougall, T. J., and P. M. Barker, 2011: Getting started with teos-10 and the gibbs seawater (gsw) oceanographic toolbox. *Scor/iapso WG*, **127 (532)**, 1–28.

Nie, X., S. Gao, F. Wang, J. Chi, and T. Qu, 2019: Origins and pathways of the pacific equatorial undercurrent identified by a simulated adjoint tracer. *Journal of Geophysical Research: Oceans*, **124 (4)**, 2331–2347, https://doi.org/doi.org/10.1029/2018JC014212.

Oort, A. H., L. A. Anderson, and J. P. Peixoto, 1994: Estimates of the energy cycle of the oceans. *Journal of Geophysical Research: Oceans*, **99 (C4)**, 7665–7688, https://doi.org/doi.org/10.1029/93JC03556.

Perez, R. C., and W. S. Kessler, 2009: Three-dimensional structure of tropical cells in the central equatorial pacific ocean. *Journal of Physical Oceanography*, **39 (1)**, 27–49, https://doi.org/doi.org/10.1175/2008JPO4029.1.

Saenz, J. A., R. Tailleux, E. D. Butler, G. O. Hughes, and K. I. Oliver, 2015: Estimating lorenz's reference state in an ocean with a nonlinear equation of state for seawater. *Journal of Physical Oceanography*, **45 (5)**, 1242–1257, https://doi.org/doi.org/10.1175/JPO-D-14-0105.1.

Seager, R., M. Cane, N. Henderson, D.-E. Lee, R. Abernathey, and H. Zhang, 2019: Strengthening tropical pacific zonal sea surface temperature gradient consistent with rising greenhouse gases. *Nature Climate Change*, **9 (7)**, 517–522, https://doi.org/doi.org/10.1038/s41558-019-0505-x.

Seager, R., N. Henderson, and M. Cane, 2022: Persistent discrepancies between observed and modeled trends in the tropical pacific ocean. *Journal of Climate*, **35 (14)**, 4571–4584, https://doi.org/doi.org/10.1175/JCLI-D-21-0648.1.

Shi, J., A. V. Fedorov, and S. Hu, 2020: A sea surface height perspective on el niño diversity, ocean energetics, and energy damping rates. *Geophysical Research Letters*, **47 (7)**, e2019GL086 742, https://doi.org/doi.org/10.1029/2019GL086742.

Tailleux, R., 2013: Available potential energy density for a multicomponent boussinesq fluid with arbitrary nonlinear equation of state. *Journal of Fluid Mechanics*, **735**, 499–518, https://doi.org/doi.org/10.1017/jfm.2013.509.

Tailleux, R., 2018: Local available energetics of multicomponent compressible stratified fluids. *Journal of Fluid Mechanics*, **842**, R1, https://doi.org/doi.org/10.1017/jfm.2018.196.

Turner, J., 1969: Buoyant plumes and thermals. *Annual Review of Fluid Mechanics*, **1 (1)**, 29–44, https://doi.org/doi.org/10.1146/annurev.fl.01.010169.000333.

Vecchi, G. A., and B. J. Soden, 2007: Global warming and the weakening of the tropical circulation. *Journal of Climate*, **20 (17)**, 4316–4340, https://doi.org/doi.org/10.1175/JCLI4258.1.

Vecchi, G. A., B. J. Soden, A. T. Wittenberg, I. M. Held, A. Leetmaa, and M. J. Harrison, 2006: Weakening of tropical pacific atmospheric circulation due to anthropogenic forcing. *Nature*, **441 (7089)**, 73–76, https://doi.org/doi.org/10.1038/nature04744.

Winters, K. B., P. N. Lombard, J. J. Riley, and E. A. D'Asaro, 1995: Available potential energy and mixing in density-stratified fluids. *Journal of Fluid Mechanics*, **289**, 115–128, https://doi.org/doi.org/10.1017/S002211209500125X.

Wong, K., R. Tailleux, and S. L. Gray, 2016: The computation of reference state and ape production by diabatic processes in an idealized tropical cyclone. *Quarterly Journal of the Royal Meteorological Society*, **142 (700)**, 2646–2657, https://doi.org/doi.org/10.1002/qj.2854.

Wyrtki, K., 1981: An estimate of equatorial upwelling in the pacific. *Journal of Physical Oceanography*, **11 (9)**, 1205–1214, https://doi.org/doi.org/10.1175/1520-0485(1981)011⟨1205:AEOEUI⟩2.0.CO;2.

Xie, S.-P., C. Deser, G. A. Vecchi, J. Ma, H. Teng, and A. T. Wittenberg, 2010: Global warming pattern formation: Sea surface temperature and rainfall. *Journal of Climate*, **23 (4)**, 966–986, https://doi.org/doi.org/10.1175/2009JCLI3329.1.

Zebiak, S. E., and M. A. Cane, 1987: A model el niñ–southern oscillation. *Monthly Weather Review*, **115 (10)**, 2262–2278, https://doi.org/doi.org/10.1175/1520-0493(1987)115⟨2262:AMENO⟩2.0.CO;2.